Journal of Power Sources 269 (2014) 117–123

Contents lists available at ScienceDirect

Journal of Power Sources

journal homepage: www.elsevier.com/locate/jpowsour

Effect of high oxygen reduction reaction activity of octahedral PtNi nanoparticle electrocatalysts on proton exchange membrane fuel cell performance

Ryogo Sakamoto*, Kaoru Omichi, Terumi Furuta, Masao Ichikawa

Honda R&D Co., Ltd., Fundamental Technology Research Center, 1-4-1 Chuo, Wako-shi, Saitama, Japan

HIGHLIGHTS

- We synthesized octahedral PtNi nanoparticles catalysts for a cathode of PEMFCs.
- Nearly all surfaces of the octahedral PtNi NPs were identified as (111) facets.
- Mass activity of octahedral PtNi NPs in PEMFC was 3.4 times higher than that of commercial Pt catalysts.
- In 0.6–0.9 V potential cycling test, the octahedral PtNi NPs maintained high ORR activity.

GRAPHICAL ABSTRACT

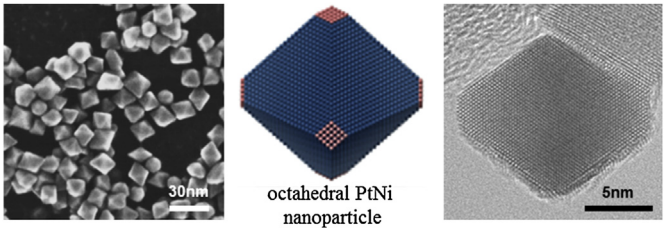

ARTICLE INFO

Article history:
Received 14 March 2014
Received in revised form
20 May 2014
Accepted 2 July 2014
Available online 9 July 2014

Keywords:
PEM fuel cell
Electrocatalysts
Octahedral PtNi nanoparticles
Oxygen reduction reaction

ABSTRACT

To reduce Pt loading in proton exchange membrane (PEM) fuel cells, we synthesized (111) faceted octahedral PtNi nanoparticles supported by carbon black (octahedral PtNi NPs/C) using a new chemical method, and evaluated the effect of reduction of Pt loading and durability in actual PEM fuel cells. We confirmed that the synthesized particles were octahedral and the PtNi alloy nanoparticles had a size of 10–15 nm. In high resolution transmission electron microscopy analysis, nearly all exposed surfaces of the octahedral PtNi NPs were identified as (111) facets. Energy dispersion X-ray spectroscopy analysis showed that the corners and edges of the octahedral PtNi NPs were richer in platinum than the internal region, thus it was determined that the octahedral PtNi NPs adopted a core–shell structure. Mass activity of octahedral PtNi NPs/C as a cathode in fuel cells was 3.4 times higher than that of commercial Pt catalysts. This corresponds to a 71% reduction of Pt for the cathode. In potential cycling tests, the octahedral PtNi NPs/C also exhibited better durability than the commercial Pt catalysts.

1. Introduction

Proton exchange membrane (PEM) fuel cells are clean energy systems and are expected to be applied to future vehicles. One of the main issues for the development of practical PEM fuel cells for vehicles is the cost. In cathodes of PEM fuel cells, large amounts of Pt are used to obtain sufficient oxygen reduction reaction (ORR) activity. This is the major cause of the high cost of PEM fuel cells, and is undesirable in terms of resource risk. Reducing Pt loading in cathodes is therefore essential.

Increasing the ORR mass activity of Pt represents a highly effective means of reducing the Pt loading in the cathode. A number of approaches, e.g., Pt-alloying [1–8], core–shell structures [9–14] and crystal faces-controlled structures [15–19], have been

* Corresponding author. Tel.: +81 48 461 2511; fax: +81 48 462 5330.
E-mail addresses: ryogo_sakamoto@n.f.rd.honda.co.jp, ryogo@bk2.so-net.ne.jp (R. Sakamoto).

http://dx.doi.org/10.1016/j.jpowsour.2014.07.011
0378-7753/

proposed and investigated. Among these it was reported that orientation-controlled crystals showed very high ORR activity. Markovic et al. reported that the ORR activity of single-crystal Pt increases corresponding to (100) < (111) < (110) [15]. In contrast, Stamenkovic et al. showed a difference for single-crystal Pt_3Ni alloys, in which the order of increasing ORR activity is (100) < (110) < (111) [16]. It was also found that the ORR activity of Pt_3Ni(111) was 10 times higher than that of Pt(111). These findings indicate that alloying and crystal orientation may in combination affect a very large increase in the ORR activity.

It is important to note that all of these reports were based on investigations of single-crystal electrodes. In an actual fuel cell, it is necessary to apply electrocatalysts with high specific surface areas to obtain high ORR activity for a small catalyst quantity. To achieve high specific surface area, synthesis of nanoparticles is one of the most effective approaches. In this light, we chose to synthesize octahedral PtNi nanoparticles, which are enclosed by PtNi(111) facets, supported by carbon black (octahedral PtNi NPs/C) in a process of slow nanocrystal growth, using polyol reduction with poly(diallyldimethylammonium chloride) (PDDA). Octahedral PtNi NPs/C has been shown to exhibit substantially higher ORR activity than Pt catalysts in Rotating Disc Electrode (RDE) measurements [17–19], however no evaluation of actual fuel cell performance and durability has been reported. In this report, we synthesized octahedral PtNi NPs/C by a new chemical method, performed fuel cell tests to examine their effect in reducing Pt loading in cathodes, and evaluated their durability.

2. Experimental

2.1. Synthesis of octahedral PtNi NPs/C

Octahedral PtNi NPs/C was synthesized by a simple chemical method as follows. In a 300-mL three-necked flask with ethylene glycol (50 mL) (Kanto Chemical), Ketjenblack ECP-600JD (513 mg) (Lion Corporation), platinum acetylacetonate (588 mg) (Aldrich), nickel acetate tetrahydrate (372 mg) (Aldrich) and 35 wt.% PDDA aqueous solution (760 μL) (Aldrich) were added and refluxed under an Ar gas flow. After standing for 2 h at 190 °C, the product was separated from the reaction liquid by filtration, washed several times in hot ethanol, acetone, and water, and then thoroughly dried at 50 °C, thus affording the octahedral PtNi NPs/C.

2.2. Physical characterization

Scanning electron microscopy (SEM) and transmission electron microscopy (TEM) images of octahedral PtNi NPs/C were obtained by a Hitachi High-Tech HD-2000 (accelerating voltage 200 kV) equipped with an energy dispersion X-ray spectrometer (EDX). High-resolution TEM characterization was performed by a Hitachi High-Tech H-9000UHR (accelerating voltage 300 kV). X-ray diffraction (XRD) patterns were collected on a Bruker D8 ADVANCE using Cu-Kα radiation.

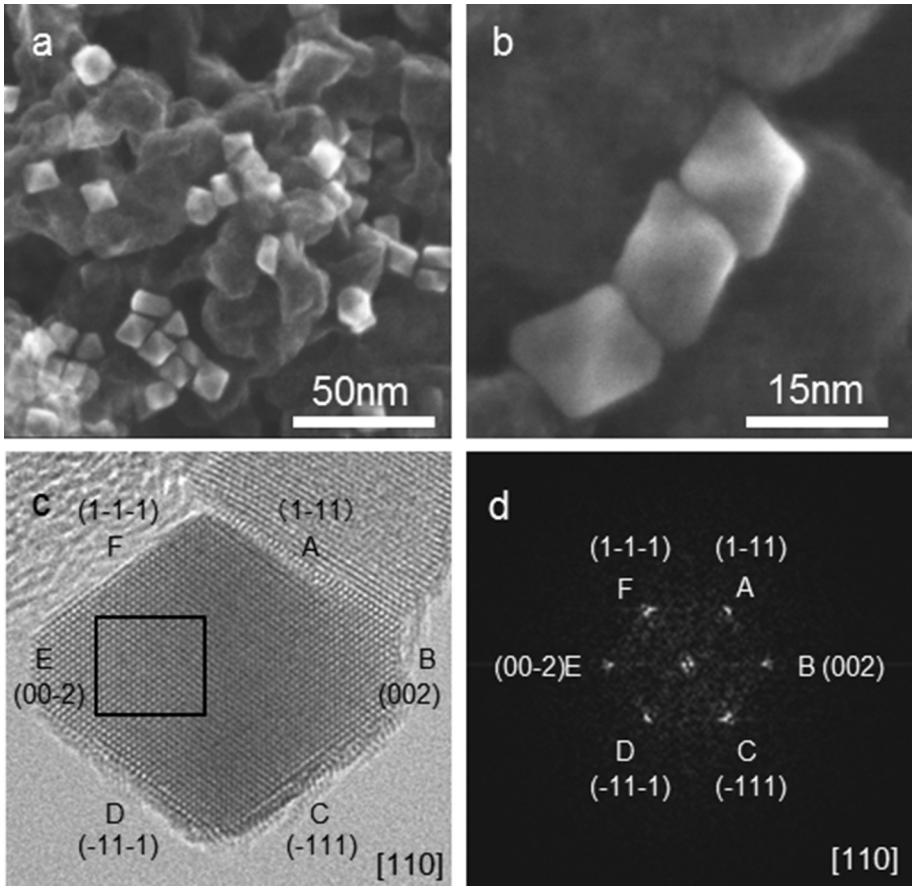

Fig. 1. (a and b) SEM and (c) high-resolution TEM images of octahedral PtNi NPs/C. The square shows the area image-processed by inverse Fourier transformation to obtain the pseudo electron diffraction pattern. (d) Pseudo electron diffraction pattern of octahedral PtNi nanoparticles.

2.3. Electrochemical evaluations

To perform RDE measurements, a catalyst film of the octahedral PtNi NPs/C was prepared as follows. The octahedral PtNi NPs/C was added to a mixture of aqueous ethanol and 5 wt.% Nafion® solution (Aldrich) and dispersed ultrasonically. The ink was dropped on a glassy carbon electrode (5 mm diameter) and dried in air at room temperature. The amount of Pt on the electrode was determined gravimetrically. The RDE measurement of the octahedral PtNi NPs/C (Pt:1.5 μg) was carried out using an RDE apparatus (Princeton Applied Research) and a six-necked electrochemical cell with a Pt counter electrode and a saturated calomel reference electrode in O_2-saturated aqueous 0.1 M $HClO_4$ solution. The rotation rate was 2000 rpm. The potential range was from 0.015 to 1.05 V (vs. RHE) at 5 mV s^{-1} using an electrochemical measurement system (Solartron SI1287). To obtain the electrochemical surface area (ECSA) of the octahedral PtNi NPs/C on the electrode, cyclic voltammogram (CV) measurements were performed in Ar-saturated aqueous 0.1 M $HClO_4$. The ECSA was calculated from the hydrogen adsorption charge area (0.05–0.40 V) as 0.21 mC cm^{-2}. For comparison, RDE measurements and CV measurements of a commercial carbon-supported Pt catalyst (Pt/C) (Pt: 3.9 μg) were similarly performed.

A membrane-electrode-assembly (MEA) of the octahedral PtNi NPs/C was prepared using a general decal method. The octahedral PtNi NPs/C was mixed with ultrapure water and 5 wt.% Nafion® solution (Aldrich) by ultrasonication. The ink was then sprayed on a Teflon® sheet (30 × 30 mm) and dried to make a decal sheet for the cathode. Similarly, a decal sheet of a commercial Pt/C was prepared for the anode. A pair of the prepared decal sheets was hot-pressed on a Nafion® membrane (NR-212) to make an MEA. Both the layer size of anode and cathode on MEA were 30 × 30 mm (9 cm^2). The Pt loading of the cathode and anode were 0.14 mg cm^{-2} and 0.50 mg cm^{-2}, respectively. The prepared MEA and gas diffusion layers (SGL carbon) were set to a Japan Automobile Research Institute (JARI) standard cell, and it was attached to fuel cell testing system (NF Corporation). For electrochemical cleaning of MEA to bring out the fuel cell performance fully, polarization cycles that called "cell-aging process" were performed repeatedly. The conditions of cell-aging process were same as fuel cell tests that were described below. After the cell-aging process was done fully, actual fuel cell tests were performed with conditions below. The cell temperature was 70 °C. The anode and the cathode gases were H_2 and air, humidified at 50% and 73% relative humidity, controlled at a gas stoichiometric ratio of 1.4 and 1.8, and a backpressure of 130 kPa and 100 kPa, respectively. For comparison, an MEA with the commercial Pt/C for both electrodes, whose Pt loadings were both 0.50 mg cm^{-2}, was prepared, and fuel cell tests were performed with the same conditions as above.

To assess the durability of octahedral PtNi NPs/C in the fuel cell, before and after the potential cycling, fuel cell tests were performed. The cell conditions were similar to the above fuel cell tests except that both anode H_2 gas and cathode air were fully humidified. Square-shaped potential waves were applied to the cell 10,000 times between 0.6 V and 0.9 V using a potentiostat (Hokuto Denko HD-3000). The potential was maintained for 20 s at each potential. Before and after the cycling, CV measurements were performed to check the changes of ECSA in the cathode by filling the cathode side with N_2 gas.

3. Results and discussion

3.1. Physical characterization of octahedral PtNi NPs/C

Fig. 1 shows SEM and TEM images of the octahedral PtNi NPs/C. The low-magnification SEM image of Fig. 1(a) shows well-dispersed octahedral particles on carbon black with particle sizes of 10–15 nm. As seen in the high-magnification SEM image of Fig. 1(b), the nanoparticles are not perfect octahedrons but rather truncated octahedrons. Fig. 1(c) shows a high-resolution TEM image of the octahedral PtNi NPs along the [110] direction. Fig. 1(d) shows the pseudo electron diffraction pattern image obtained by fast Fourier transformation, the diffraction spot of which was indexed for the area enclosed by the square in Fig. 1(c). The surfaces with cut corners (B, E) in Fig. 1(c) were identified as (100) facets and the others (A, C, D, F) as (111) facets, thus nearly all exposed surfaces of the octahedral PtNi NPs were identified as (111) facets.

There are two important factors in obtaining (111) faceted octahedral PtNi NPs/C. The first is the effect of PDDA as a capping agent. PDDA is a polymer with high density functional groups that serve as adsorption sites, and therefore exhibits extremely strong absorptivity [20,21]. In the reactions, PDDA coordinates with Pt^{2+} and Ni^{2+} ions, inhibiting their reduction to Pt(0) and Ni(0) atoms, thus slowing the nucleation reaction and limiting the number of nuclei formed. The precursors are consumed in the particle growth, and uniform particle growth occurs at the atomic level by continuous metal deposition, thus resulting in the formation of larger particles with a comparatively large proportion of facets compared to corners and edges. The second factor is that PtNi(111) facets have lower surface energy than the other facets [17,22–24]. The growth rate of crystal faces with low surface energy is comparatively slow, thus the proportion of the crystal faces exposed becomes large. Furthermore, selective PDDA adsorption to PtNi(111) may further

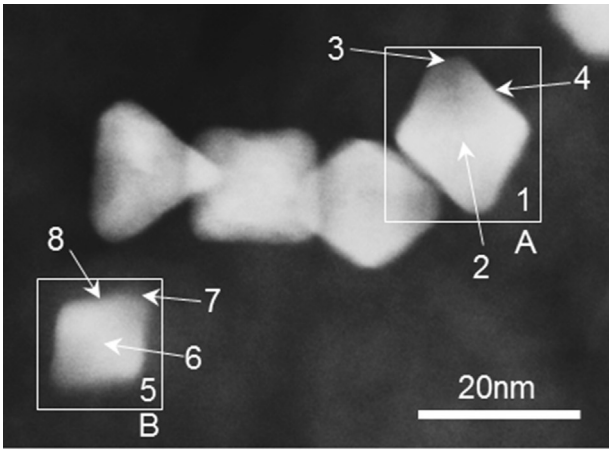

Analysis points		Pt:Ni /at.%
1	particle	63.8 : 36.2
2	center	57.3 : 42.7
3	corner	80.7 : 19.3
4	edge	72.3 : 27.7
5	particle	67.2 : 32.8
6	center	80.8 : 19.2
7	corner	58.1 : 41.9
8	edge	73.6 : 26.4

Fig. 2. Dark-field SEM image of octahedral PtNi NPs/C including EDX analysis areas (squares) and points (arrows).

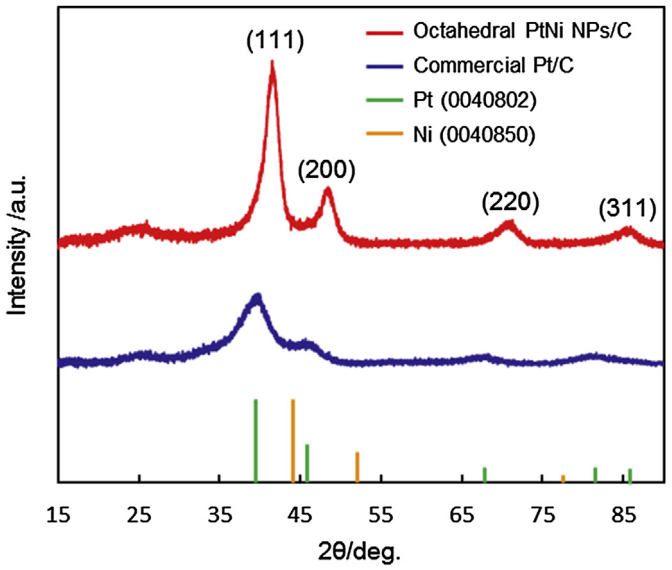

Fig. 3. XRD patterns for octahedral PtNi NPs/C and commercial Pt/C, and the theoretical peaks for Pt(0040802) and Ni(0040850).

lower its surface energy. We believe that these combined effects enabled the formation of octahedral PtNi nanoparticles.

Fig. 2 shows the local atomic compositions of two of the octahedral PtNi NPs obtained by EDX. The overall (analysis points-1) composition of particle A is Pt:Ni = 63.8:36.2, indicating it is rich in platinum. The compositional ratio in the center (analysis points-2) of particle A is Pt:Ni = 57.3:42.7 in contrast to the values of Pt:Ni = 80.7:19.3 at the corner (analysis points-3) and Pt:Ni = 72.3:27.7 at the edge (analysis points-4). These results clearly indicate that the corners and edges of the octahedral PtNi NPs are richer in platinum than the internal region. The compositional distribution of particle B shows a similar tendency. These results indicate that the octahedral PtNi NPs adopt a core–shell structure.

Fig. 3 shows the XRD patterns of the octahedral PtNi NPs/C and the commercial Pt/C. The XRD pattern of the octahedral PtNi NPs/C is the same as the characteristic pattern of pure Pt in relative peak positions and intensity ratios, thus showing it to have the same fcc structure as Pt. The diffraction peaks of the octahedral PtNi NPs/C are shifted toward the high-angle side relative to those of the commercial Pt/C, which is due to shortening of the crystal face interval by alloying the Pt with Ni. The difference between the commercial Pt/C and the octahedral PtNi NPs/C in (111) peak-top position is 1.65°. This difference indicates that the crystal face interval in the (111) direction is 0.085 Å shorter than that of the commercial Pt/C. The diffraction peaks of the octahedral PtNi NPs/C are also asymmetrical. The top of each peak is shifted toward the high-angle side, with a shoulder on the low-angle side. We consider that the asymmetric peaks and the shoulders on the low-angle side are due to the atomic compositional distribution of the octahedral PtNi NPs shown in Fig. 2.

3.2. Electrochemical evaluations

Fig. 4(a) shows polarization curves of octahedral PtNi NPs/C (Pt: 1.5 μg) and commercial Pt/C (Pt: 3.9 μg) by RDE measurements. Fig. 4(b) shows Tafel plots of both electrocatalysts. The currents of Tafel plots were normalized by Pt loading and converted to remove

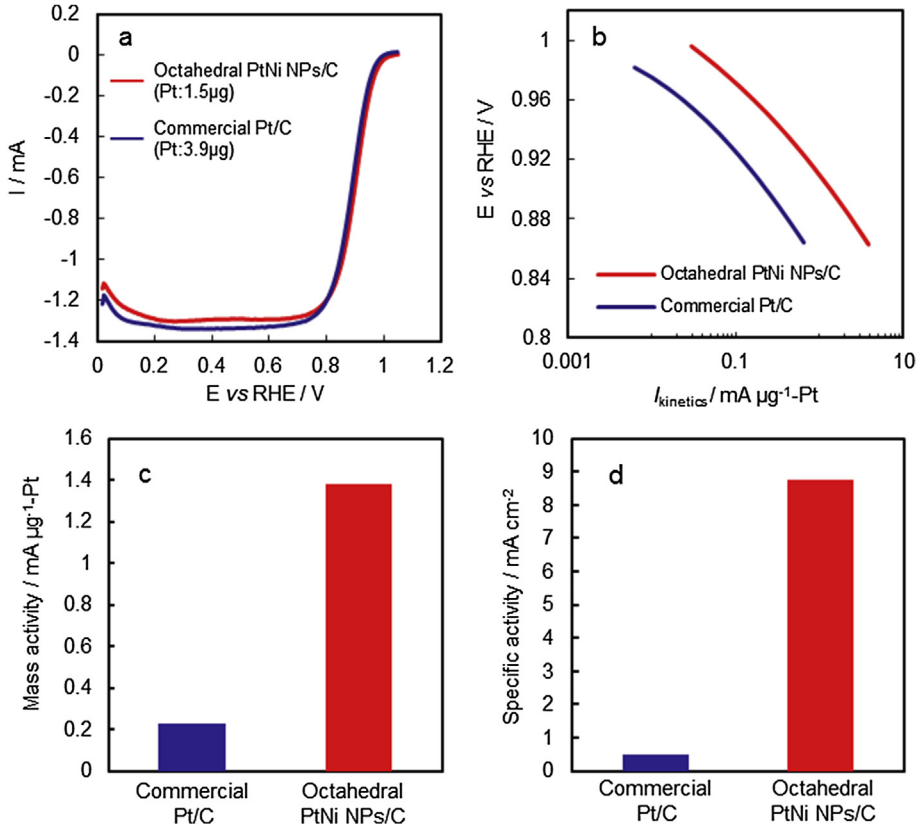

Fig. 4. (a) Polarization curves and (b) Tafel plots of octahedral PtNi NPs/C (Pt:1.5 μg) and commercial Pt/C (Pt:3.9 μg) by RDE measurements. The currents of Tafel plots were normalized by Pt loading and converted to remove the influence of the diffusion of oxygen in the electrolyte. (c) Comparison of ORR mass activity and (d) specific activity at 0.90 V (vs. RHE) between octahedral PtNi NPs/C and commercial Pt/C.

the influence of the diffusion of oxygen in the electrolyte. Fig. 4(c) shows the comparison of mass activity of both electrocatalysts at 0.90 V from Tafel plots. The mass activity of octahedral PtNi NPs/C is about 6.0 times higher than that of commercial Pt/C. This mass activity is the same as or more than that of previous reports [17–19]. This high ORR activity indicates the possibility of up to 83% reduction of Pt loading in the cathode using octahedral PtNi NPs/C. Fig. 4(d) shows the comparison of specific activity calculated with ECSA of both electrocatalysts at 0.90 V. The specific activity of octahedral PtNi NPs/C is about 17.9 times higher than that of commercial Pt/C, much higher than the mass activity. This suggests that the intrinsic ORR activity of octahedral PtNi without considering surface area is extremely high compared to pure Pt.

The catalytic activity and stability of octahedral PtNi NPs/C were evaluated in actual PEM fuel cell tests. Fig. 5(a) shows the polarization curves of the PEM fuel cell using the octahedral PtNi NPs/C in the cathode. In these polarization curves, despite the fact that Pt loading of octahedral PtNi NPs/C on the cathode is smaller than that of commercial Pt/C (0.14 mg-Pt cm^{-2} and 0.50 mg-Pt cm^{-2}, respectively), both fuel cell performances are almost the same. To evaluate the Pt-mass activity of octahedral PtNi NPs/C in actual PEM fuel cell, Tafel plots that normalized by Pt loading are represented in Fig. 5(b), and the mass activity of octahedral PtNi NPs/C at 0.90 V is compared to that of commercial Pt/C in Fig. 5(c). As shown in Fig. 5(c), the mass activity at 0.90 V of the octahedral PtNi NPs/C is 3.4 times higher than that of the commercial Pt/C in PEM fuel cell tests. These results indicate that by using the octahedral PtNi NPs/C as a substitute for commercial Pt/C, a 71% reduction of Pt loading in the cathode of PEM fuel cells will be possible. Thus it was shown that octahedral PtNi NPs/C has great potential to reduce the cost of PEM fuel cells.

The ratios of mass activity in the PEM fuel cell for the octahedral PtNi NPs/C and the commercial Pt/C are smaller than that in the RDE measurements. The reasons for this are currently being studied. However, we expect one of them is the presence of residual PDDA in the cathode of the MEA. If the residual PDDA was on octahedral PtNi NPs, it may reduce the number of the active sites and inhibit ORR. In the RDE measurements, the electrodes were immersed in an aqueous electrolyte, and PDDA, which is highly soluble in water, should be presumably dissolved in the electrolyte. Moreover, in the electrochemical cleaning by potential cycling prior to the polarization test, any PDDA adsorbed strongly to the particle surfaces should have been removed. This would permit an exertion of the ORR activity of the octahedral PtNi NPs/C. In the PEM fuel cell tests, in contrast, the cell-aging process was performed by polarization cycling with the electrodes surrounded by gases rather than liquids. Therefore, the PDDA removal effect by the cell-aging process may be smaller. We expect that this may be a major cause of smaller mass activity of the octahedral PtNi NPs/C in the PEM fuel cell.

Fig. 6(a) shows the polarization curves of the octahedral PtNi NPs/C in the PEM fuel cell before and after 10,000 cycles of the potential cycle of 0.6–0.9 V. No substantial loss in fuel cell performance is found in any current region. As shown in Fig. 6(b), the declining rate of the mass activity before and after the potential cycling for the commercial Pt/C and the octahedral PtNi NPs/C are 29% and 19%, respectively. Thus it is found that the durability of the octahedral PtNi NPs/C in the 0.6–0.9 V potential cycle is superior to

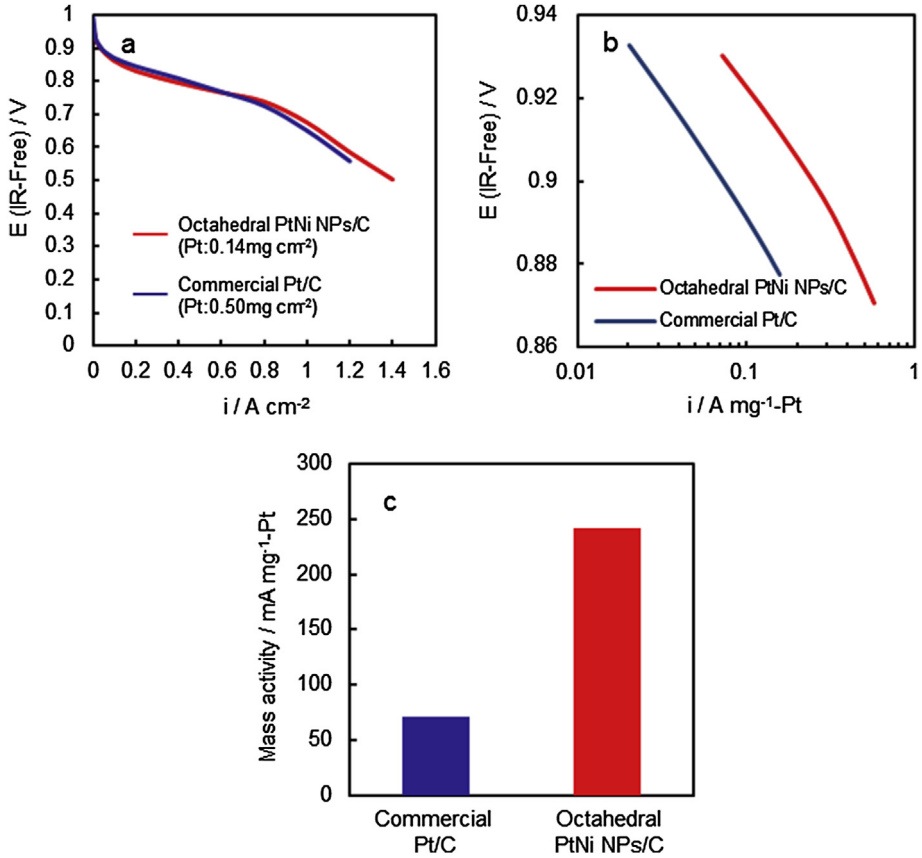

Fig. 5. (a) Polarization curves of PEM fuel cells with octahedral PtNi NPs/C or commercial Pt/C for cathodes. (b) Tafel plots of octahedral PtNi NPs/C and commercial Pt/C for PEM fuel cell tests. (c) Mass activity at 0.90 V of the octahedral PtNi NPs/C and commercial Pt/C.

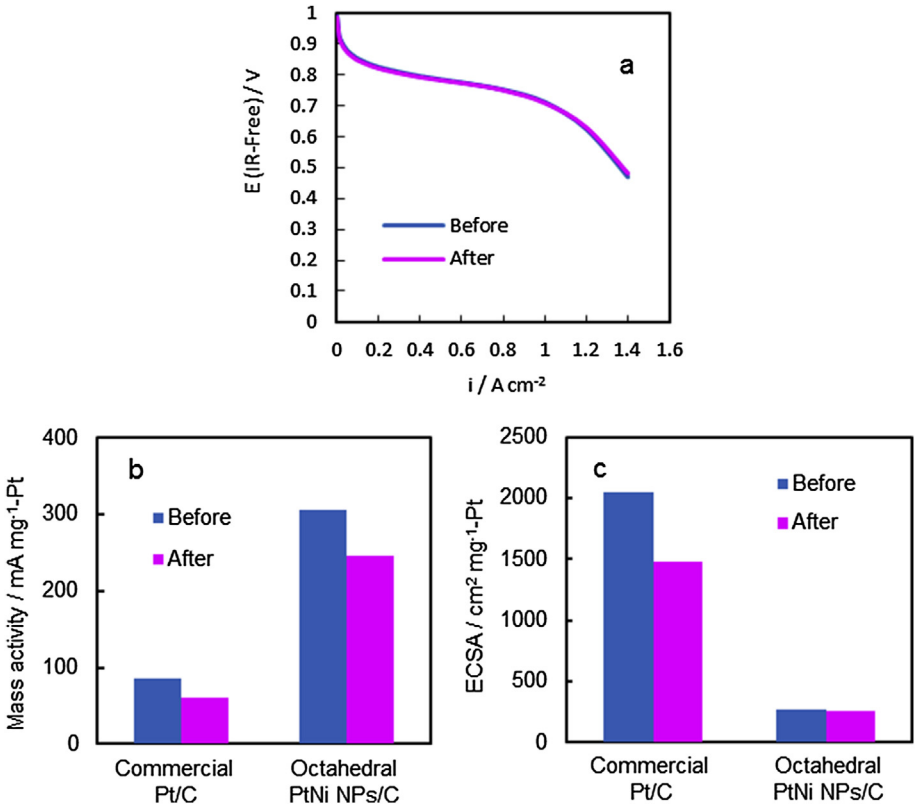

Fig. 6. (a) Polarization curves of octahedral PtNi NPs/C before and after 10,000 potential cycles of 0.6–0.9 V in fuel cell test. (b) Change of mass activity and (c) ECSA of octahedral PtNi NPs/C and commercial Pt/C before and after the 0.6–0.9 V potential cycling.

that of the commercial Pt/C. Furthermore, the mass activity of the octahedral PtNi NPs/C after the potential cycling remains 4.1 times higher than that of the commercial Pt/C.

We consider that the reason of better durability of the octahedral PtNi NPs/C should be due to its small changing of ECSA during the durability tests. Fig. 6(c) shows the ECSA of electrocatalysts in cathodes before and after the potential cycling. The declining rate of ECSA for the commercial Pt/C and the octahedral PtNi NPs/C are 28% and 4%, respectively. For the commercial Pt/C, the declining rate of ECSA is about the same as its activity loss ratio (29%). This indicates that the main cause of the activity loss in the potential cycling for the commercial Pt/C is a decrease in surface area of the Pt nanoparticles. For the octahedral PtNi NPs/C, the declining rate of ECSA was very small, thus that was not main cause of the activity loss. In general, a decreasing of ECSA of nano-electrocatalysts by fuel cell operation results from Ostwald ripening, which is due to their surface oxidation, dissolution and re-deposition of atomic metals. The octahedral PtNi NPs may be resistant to Ostwald ripening, thus its declining rate of ECSA was very small, and they showed better durability. We examine there may be two reasons why Ostwald ripening didn't proceed so fast. The first is that the size of the octahedral PtNi NPs was relatively large. As shown in Fig. 1(a) and (b), the size of the octahedral PtNi NPs was ~15 nm, and larger than that of the commercial Pt NPs (~3 nm). It has been reported that Ostwald ripening for smaller particles progresses faster [25]. The second is that the surface of octahedral PtNi NPs has high stability because of Pt-rich (111) facets. As shown in Fig. 1(c) and Fig. 2, almost all the surfaces of octahedral PtNi NPs were identified as Pt-rich (111) facets. Because the (111) facet is high in both atomic density and atomic coordination number, we believe it should be relatively more resistant to dissolution from surface than the other facets.

The causes of 19% activity loss of the octahedral PtNi NPs/C by durability tests are under investigations. We recognize that the changing of atomic composition due to dissolution of Ni from inside of the octahedral PtNi NPs and losing of (111) facets that produce high ORR activity are important concerns.

4. Conclusion

To reduce Pt loading in PEM fuel cells, we have synthesized (111) faceted octahedral PtNi nanoparticles supported by carbon black (octahedral PtNi NPs/C) using a new chemical method, and evaluated their ORR activity and durability by RDE measurements and actual fuel cell tests. We confirmed that the synthesized particles were octahedral with PtNi alloy nanoparticles of size 10–15 nm by SEM. In high resolution TEM analysis, nearly all exposed surfaces of the octahedral PtNi NPs were identified as (111) facets. The SEM-EDX analysis showed that the corners and edges of the octahedral PtNi NPs were richer in platinum than the internal region, thus it was found that the octahedral PtNi NPs adopted a core–shell structure. In evaluations of ORR activity of the octahedral PtNi NPs/C by RDE measurements, mass and specific activities were 6.0 and 17.9 times higher than those of the commercial Pt/C, respectively. MEAs using the octahedral PtNi NPs/C in the cathode were prepared and evaluated by actual fuel cell performances and durability. Mass activity of octahedral PtNi NPs/C on the cathode was 3.4 times higher than that of commercial Pt/C. This indicated that a 71% reduction of Pt for the cathode would be possible. In durability tests by 0.6–0.9 V potential cycling, there was almost no variation of the polarization curves before and after 10,000 cycles. We believe that the octahedral PtNi NPs/C has great potential to reduce the Pt loading in PEM fuel cells.

References

[1] V.R. Stamenkovic, B.S. Mun, M. Arenz, K.J.J. Mayrhofer, C.A. Lucas, G. Wang, P.N. Ross, N.M. Markovic, Nat. Mater. 6 (2007) 241–247.
[2] A.B. Anderson, J. Roques, S. Mukerjee, V.S. Murthi, N.M. Markovic, V. Stamenkovic, J. Phys. Chem. B 109 (2005) 1198–1203.
[3] U.A. Paulus, A. Wokaun, G.G. Scherer, T.J. Schmidt, V. Stamenkovic, V. Radmilovic, N.M. Markovic, P.N. Ross, J. Phys. Chem. B 106 (2002) 4181–4191.
[4] S. Chen, P.J. Ferreira, W. Sheng, N. Yabuuchi, L.F. Allard, Y. Shao-Horn, J. Am. Chem. Soc. 130 (2008) 13818–13819.
[5] E. Antolini, J.R.C. Salgado, E.R. Gonzalez, J. Power Sources 160 (2006) 957–968.
[6] H. Wu, D. Wexler, G. Wang, J. Alloys Compd. 488 (2009) 195–198.
[7] L. Xiong, A. Manthiram, Electrochim. Acta 50 (2005) 2323–2329.
[8] L. Xiong, K.L. More, T. He, J. Power Sources 195 (2010) 2570–2578.
[9] J. Zhang, F.H.B. Lima, M.H. Shao, K. Sasaki, J.X. Wang, J. Hanson, R.R. Adzic, J. Phys. Chem. B 109 (2005) 22701–22704.
[10] F. Tao, M.E. Grass, Y. Zhang, D.R. Butcher, J.R. Renzas, Z. Liu, J.Y. Chung, B.S. Mun, M. Salmeron, G.A. Somorjai, Science 322 (2008) 932–934.
[11] K. Sasaki, H. Naohara, Y. Cai, Y.M. Choi, P. Liu, M.B. Vukmirovic, J.X. Wang, R.R. Adzic, Angew. Chem. Int. Ed. 49 (2010) 8602–8607.
[12] K. Sasaki, J.X. Wang, H. Naohara, N. Marinkovic, K. More, H. Inada, R.R. Adzic, Electrochim. Acta 55 (2010) 2645–2652.
[13] M. Shao, K. Sasaki, N. Marinkovic, L. Zhang, R. Adzic, Electrochem. Commun. 9 (2007) 2848–2853.
[14] P. Mani, R. Srivastava, P. Strasser, J. Phys. Chem. C 112 (2008) 2770–2778.
[15] N.M. Marković, R.R. Adžić, B.D. Cahan, E.B. Yeager, J. Electroanal. Chem. 377 (1994) 249–259.
[16] V.R. Stamenkovic, B. Fowler, B.S. Mun, G. Wang, P.N. Ross, C.A. Lucas, N.M. Markovic, Science 315 (2007) 493–497.
[17] J. Zhang, H. Yang, J. Fang, S. Zou, Nano Lett. 10 (2010) 638–644.
[18] C. Cui, L. Gan, H.-H. Li, S.-H. Yu, M. Heggen, P. Strasser, Nano Lett. 12 (2012) 5885–5889.
[19] M.K. Carpenter, T.E. Moylan, R.S. Kukreja, M.H. Atwan, M.M. Tessema, J. Am. Chem. Soc. 134 (2012) 8535–8542.
[20] Z.Q. Tian, S.P. Jiang, Z. Liu, L. Li, Electrochem. Commun. 9 (2007) 1613–1618.
[21] Z. Liu, S. Koh, C. Yu, P. Strasser, J. Electrochem. Soc. 154 (2007).
[22] B.S. Mun, M. Watanabe, M. Rossi, V. Stamenkovic, N.M. Markovic, P.N. Ross, J. Chem. Phys. 123 (2005).
[23] J.R. Kitchin, J.K. Nørskov, M.A. Barteau, J.G. Chen, J. Chem. Phys. 120 (2004).
[24] N. Tian, Z.Y. Zhou, S.G. Sun, Y. Ding, Z.L. Wang, Science 316 (2007) 732–735.
[25] Z. Xu, H. Zhang, H. Zhong, Q. Lu, Y. Wang, D. Su, Appl. Catal. B Environ. 111–112 (2012) 264–270.